GDCh

Research Articles

Angewandte
Chemie
International Edition
www.angewandte.org

VIP **Nitrides** *Very Important Paper*

High-pressure and high-temperature synthesis of crystalline Sb3N5

Matteo Ceppatelli,* Manuel Serrano-Ruiz, Marta Morana, Kamil Dziubek, Demetrio Scelta, Gaston Garbarino, Tomasz Poręba, Mohamed Mezouar, Roberto Bini, and Maurizio Peruzzini

Abstract: A chemical reaction between Sb and N_2 was induced under high-pressure (32–35 GPa) and high-temperature (1600–2200 K) conditions, generated by a laser heated diamond anvil cell. The reaction product was identified by single crystal synchrotron X-ray diffraction at 35 GPa and room temperature as crystalline antimony nitride with Sb_3N_5 stoichiometry and structure belonging to orthorhombic space group $Cmc2_1$. Only Sb–N bonds are present in the covalent bonding framework, with two types of Sb atoms respectively forming SbN_6 distorted octahedra and trigonal prisms and three types of N atoms forming NSb_4 distorted tetrahedra and NSb_3 trigonal pyramids. Taking into account two longer Sb–N distances, the SbN_6 trigonal prisms can be depicted as SbN_8 square antiprisms and the NSb_3 trigonal pyramids as NSb_4 distorted tetrahedra. The Sb_3N_5 structure can be described as an ordered stacking in the bc plane of bi- layers of SbN_6 octahedra alternated to monolayers of SbN_6 trigonal prisms (SbN_8 square antiprisms). The discovery of Sb_3N_5 finally represents the long sought-after experimental evidence for Sb to form a crystalline nitride, providing new insights about fundamental aspects of pnictogens chemistry and opening new perspectives for the high-pressure chemistry of pnictogen nitrides and the synthesis of an entire class of new materials.

Introduction

Binary crystalline nitrides of group 15 elements represent a class of elusive compounds, which has remained largely unexplored so far. The reason behind this lack of knowledge is evidently found in the challenging pressure and temperature conditions required for their synthesis, which make the effective reactive paths inaccessible to conventional ambient pressure chemistry. As a result, the absence of crystalline nitrides of group 15 elements heavier than P has always represented an open issue in inorganic chemistry.[1–3]

Indeed, until recently and for more than 20 years, the experimentally reported and structurally characterized crystalline pnictogen nitrides have been limited to α-P_3N_5, synthesized from chemical precursors at ambient pressure and high temperature,[4] and γ-P_3N_5, obtained a few years later by high-temperature compression of α-P_3N_5.[5]

However, in the last couple of years, a few experimental studies, based on the use of laser heated diamond anvil cells (DACs) to generate high-pressure (HP) and high-temperature (HT) conditions, have provided game changing advancements on this topic and established new foundations for the exploration of these elusive materials in the high-pressure domain.[6–9]

This method has not only allowed the direct synthesis of α- and γ-P_3N_5 from P and N_2 in condensed phase,[6,7] but also provided experimental evidence for the existence of a predicted crystalline P_3N_5 polymorph containing hexa-coordinated P atoms (δ-P_3N_5) and of the new pyrite-type PN_2 and α'-P_3N_5 structures.[8] The HP-HT synthesis of these compounds demonstrates the role of pressure in increasing

[*] M. Ceppatelli, D. Scelta, R. Bini
LENS, European Laboratory for Non-linear Spectroscopy, Via N. Carrara 1, I-50019 Sesto Fiorentino, Firenze, Italy
E-mail: ceppa@lens.unifi.it
      matteo.ceppatelli@iccom.cnr.it

M. Ceppatelli, M. Serrano-Ruiz, D. Scelta, R. Bini, M. Peruzzini
ICCOM-CNR, Institute of Chemistry of OrganoMetallic Compounds, National Research Council of Italy, Via Madonna del Piano 10, I-50019 Sesto Fiorentino, Firenze, Italy
E-mail: ceppa@lens.unifi.it
      matteo.ceppatelli@iccom.cnr.it

M. Morana
Dipartimento di Scienze della Terra, Università degli Studi di Firenze, Via G. La Pira 4, I-50121, Firenze, Firenze, Italy

K. Dziubek
Institut für Mineralogie und Kristallographie, Universität Wien, Josef-Holaubek-Platz 2, A-1090, Wien, Austria

G. Garbarino, T. Poręba, M. Mezouar
ESRF, European Synchrotron Radiation Facility, 71 Avenue des Martyrs, CS40220, 38043 Grenoble Cedex 9, France

R. Bini
Dipartimento di Chimica "Ugo Schiff ", Università degli Studi di Firenze, Via della Lastruccia 3, I-50019 Sesto Fiorentino, Firenze, Italy

the coordination number of P and highlights the possible existence of further crystalline nitrides of P and N.

In the last years, theoretical and computational studies have predicted the existence of new compositional spaces for crystalline inorganic nitrides,[3] indicating pnictogen nitrides specifically, among chalcogenides, other pnictides, and halides, to match the most negative cohesive energy with the highest metastability (defined as the energy above the ground state),[10] thus representing a target class of materials to be potentially synthesized under high-pressure conditions and recovered at ambient pressure as metastable materials.[10,11]

Within this context, the recent synthesis and structural characterization of crystalline single-bonded cubic arsenic nitride AsN,[9] unveiling a markedly different structural chemistry of As with N compared to lighter P, has represented a major breakthrough, opening bright new perspectives about the discovery of new structures and stoichiometries for crystalline nitrides of group 15 elements heavier than P, and making Sb, which occupies the fifth period of group 15, the key element to look at in the exploration of emerging crystalline pnictogen nitrides.

Beyond the pure advancement of fundamental chemical knowledge about the chemistry of Sb and N, understanding the stability of the Sb–N system in terms of structure, composition and metastability, is technologically relevant for the synthesis of phase change memory and thermoelectric materials[12–14] and of semiconductors for applications in optoelectronics, photovoltaics and photoelectrochemical cells.[15,16] Moreover, further interest concerns the intriguing properties predicted by calculations for the different 2D polymorphs of single layer Sb–N materials such as α-,[17] β-[18] and δ-SbN.[19,20]

Nevertheless, whereas the formation of diatomic molecular SbN units[21,22] and amorphous films of SbN,[23,24] SbN$_3$[14,24,25] and Sb$_{1-x}$N$_x$ ($x = 0.17$, 0.41, 0.45) compositions[26] has been reported in literature, excluding antimony azide Sb(N$_3$)$_3$,[27,28] to the best of our knowledge, no extended crystalline compound entirely formed by antimony and nitrogen has ever been conclusively synthesized and structurally characterized by X-ray diffraction (XRD) so far.[29] Theoretically, the increase of the chemical potential of a N-containing precursor has been proposed by Sun *et al.* as an effective route to the synthesis of new metastable inorganic crystalline materials, including antimony nitride SbN[11] and other predicted ternary nitrides.[30] Experimentally, this approach has been successfully applied to the synthesis of theoretically predicted[30] ternary nitrides Zn$_2$SbN$_3$[15] and Mg$_2$SbN$_3$,[16] in which Sb exhibits its oxidation state +5. Noticeably, Zn$_2$SbN$_3$, featuring previously unreported tetrahedrally coordinated SbN$_4$ units, represents the first synthesized ternary nitride of antimony.[15] Interestingly, the presence of excess of plasma activated N in the reaction environment likely suppresses the formation of secondary Sb phases, favoring the crystalline growth of Zn$_2$SbN$_3$.[31]

By the same method, Chen *et al.* have recently reported the transient experimental observation of a metastable layered crystalline compound formed by Sb and N, lasting 17 s at 500 °C and ambient pressure, during the rapid thermal annealing (RTA) decomposition of an amorphous antimony nitride film.[32]

However, no conclusive Rietveld refinement and structural assignment of their diffraction data was possible, with additional uncertainty introduced by the presence of layer stacking disorder. Based on first-principle crystal structure predictions Chen *et al.* proposed an orthorhombic structure with SbN composition (*Pca2$_1$*, n. 29) for the short-lived layered compound observed in their study, where Sb has oxidation state +3 in trigonal pyramidal coordination.

Interestingly, according to the calculations of Chen *et al.*,[32] whereas a compound of SbN stoichiometry containing Sb with +3 oxidation state is expected to form for positive variations of the N chemical potential between +0.78 and +1.75 eV, a compound of Sb$_3$N$_5$ stoichiometry containing Sb with oxidation state +5 could possibly form for positive variations of the N chemical potential higher than +1.75 eV.[15,32] As suggested by Sun *et al.*,[11] and demonstrated by the recent synthesis of crystalline AsN[9] and δ-P$_3$N$_5$,[8] HP-HT conditions can indeed represent effective thermodynamic handles to achieve sufficiently high values of the chemical potential of N for the activation of chemical reactivity and the formation of metastable crystalline nitrides also in the case of Sb and N.

In this respect, the *ab initio* structure search calculations performed by Lian *et al.*[33] have provided further computational insight, predicting the existence of three dynamically stable crystalline polymorphs with different stoichiometry in the compositional space of the Sb–N system at high pressure (SbN$_2$, SbN$_4$, Sb$_2$N$_3$). Each of these structures, some of them containing N$_2$ molecules at low pressure, has been predicted to undergo a sequence of phase transitions with increasing pressure, essentially leading to a higher coordination number of Sb by N: Sb$_2$N$_3$ (*Cmcm*, 100–120 GPa), SbN$_2$ (SbN$_2$-I, *C2/m*, 12–23 GPa; SbN$_2$-II, *C2/m* above 23 GPa), SbN$_4$ (SbN$_4$-I, *C2/m*, 14–31 GPa; SbN$_4$-II, $P\bar{1}$ 31–60 GPa; SbN$_4$-III, $P\bar{1}$ above 60 GPa). Noticeably, SbN$_4$, featuring higher N content, has been calculated to be a high-energy density material for the amount of released energy associated to its decomposition reaction into Sb and N$_2$.[33]

Sb and N$_2$ do not react spontaneously at ambient conditions and not even at high pressure along the room T isotherm. In this study we exploited pressure, statically generated by a membrane DAC, to increase the density and reduce the interatomic distances, and temperature, generated by laser heating, to overcome the thermodynamic and kinetic barriers and access new reactive paths. Within this approach, Sb was used as reactant and laser absorber, while N$_2$ was used as reactant and pressure transmitting medium.

A similar approach has very recently led to the HP-HT synthesis of SbCN$_3$, due to the reaction of carbon from the diamond anvils for temperature in excess of 2200 K (2200–2800 K). SbCN$_3$, containing C, N and Sb, is made of guanidinate ([CN$_3$]$^{5-}$) and Sb^{5+} ions.[34]

By this method, we report here the successful activation of a direct chemical reaction between Sb and N$_2$ in condensed phase under HP (32–35 GPa) and HT (1600–2200 K) conditions generated by a laser heated DAC and the synthesis of a crystalline nitride of antimony with Sb$_3$N$_5$

stoichiometry, whose structure was solved and refined using single crystal synchrotron XRD.

Results and Discussion

The samples containing Sb and N_2 were prepared as described in the Experimental Section SI-1. Synchrotron XRD was used to monitor the sample after loading, during compression to the laser heating (LH) pressure and after LH. No sign of reactivity was observed under room T compression in the explored pressure range up to ~50 GPa.

Before and after LH, the sample was mapped by acquiring single crystal and powder XRD patterns across a grid covering the laser heated area and the surrounding regions with 3–10 μm step resolution, depending on the sample size after reactivity. No chemical reaction between Sb and N_2 was detected when laser heating the sample to 1600 K and 15 GPa. A chemical reaction was instead repeatedly observed during different experiments, when compressing Sb in the presence of N_2 at 32–35 GPa and laser heating at this pressure at temperature between 1600 and 2200 K (Figure 1). This occurrence, observed also in the As/ N_2 system,[9] indicates the reduction of the interatomic distances to be a key factor for the activation of the chemical reaction and the formation of the reaction product along a given isotherm, suggesting the existence of a threshold pressure for the transformation. Based on existing literature data, the HP-HT conditions, at which chemical reactivity was detected, correspond to the fluid phase of Sb[35] and N_2.[36] Noticeably, also in the case of P[7] and likely in that of As,[9] reactivity with N_2 appears to take place in the fluid phase in this pressure regime.
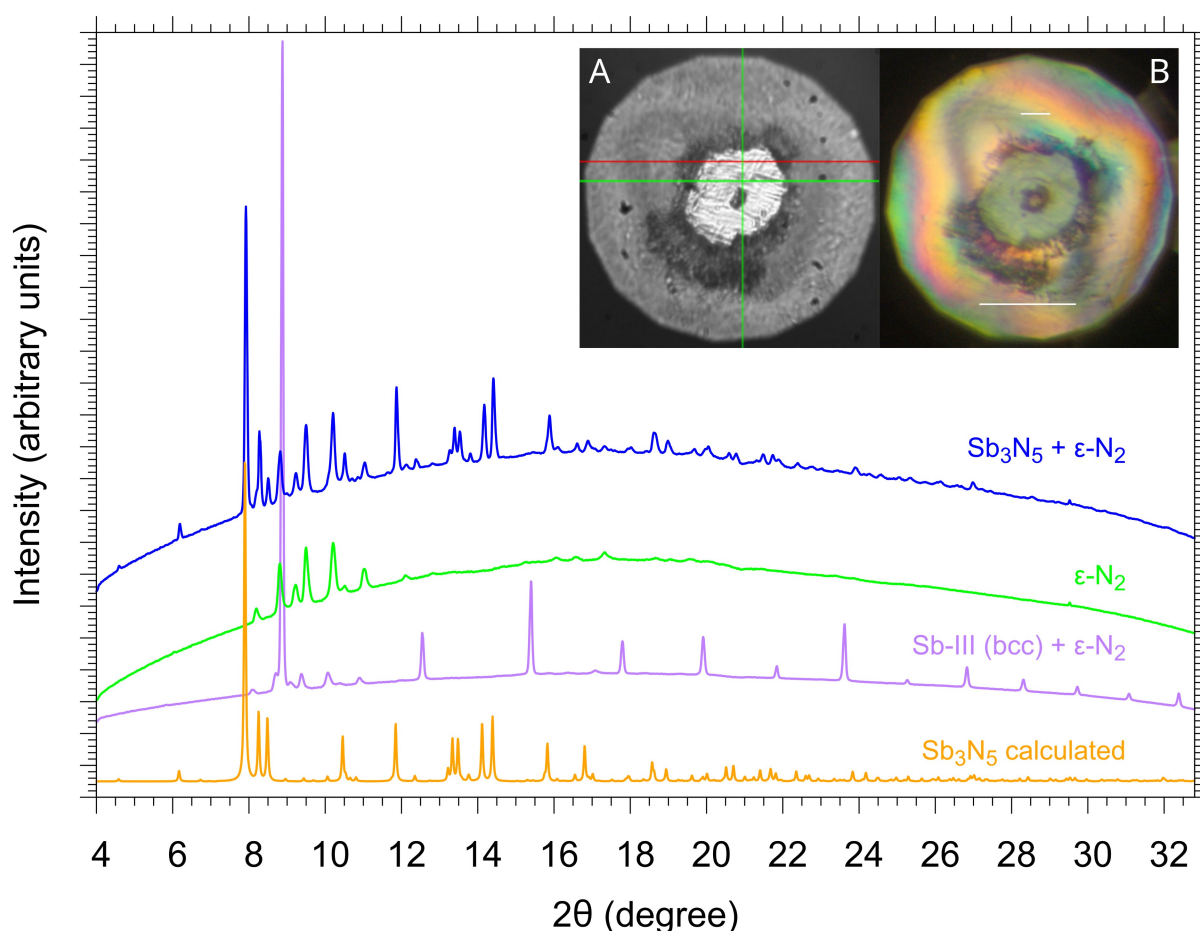

Figure 1. XRD patterns ($\lambda = 0.3738$ Å) and photomicrographs of a sample containing Sb and N_2 at room T and high pressure before and after the activation of chemical reaction upon laser heating. The photomicrographs respectively show a sample containing crystalline bcc Sb-III (central dark spot) and ε-N_2 (surrounding transparent area) at 32 GPa and room T before LH (A) and at 35 GPa and room T after LH (B). The two images, acquired using different microscopes (respectively inside (A) and outside (B) the experimental hutch of ESRF-ID27), clearly show the change in the size and shape of the initial Sb crystal after LH. Purple trace: XRD pattern acquired at 32 GPa and room T before LH at the center of the sample in the microscope image A, indicating the presence of crystalline bcc Sb-III and ε-N_2. Green trace: XRD pattern acquired in the transparent region of microscope image B at 35 GPa and room T after LH, indicating the presence of ε-N_2. Blue trace: XRD pattern acquired at the center of the laser heated area (microscope image B) at 35 GPa and room T after LH, indicating the presence of a crystalline reaction product and of excess ε-N_2. Orange trace: calculated XRD pattern using the structure obtained from single crystal data. The white scale bars on the top and bottom of photomicrograph B respectively correspond to 27 and 90 μm.

The microscope images displayed in Figure 1A and 1B, clearly showing the change in the shape and size of the starting piece of Sb after LH, provide a visual indication for the occurrence of chemical reactivity, which is confirmed by the XRD data.

The panoramic XRD patterns plotted in Figure 1 indicate that at 32 GPa and room T, before LH, the sample contains body centered cubic (bcc) Sb-III[37] and ε-N$_2$,[38] as expected at these pressure and temperature conditions (Figure 1, purple trace).

The diffraction patterns acquired after LH at the center of the laser heated area reveal instead the complete consumption of Sb-III, whose reflections completely disappeared, and the formation of a new crystalline product exhibiting distinct and sharp diffraction peaks (Figure 1, blue upper trace). Unreacted excess ε-N$_2$ can be detected after LH both at the center of the laser heated areas and in the surrounding transparent regions (Figure 1, blue and green traces).

It is worth to highlight that the reaction between Sb and N$_2$ proceeds upon LH until the complete disappearance of crystalline Sb in excess N$_2$, whereas unreacted Sb-III was found at room T in samples in which LH was reduced or intentionally stopped (Figure 2).

The analysis of the diffraction data allowed to select and identify single crystal domains, which indicate the formation of a crystalline reaction product with Sb$_3$N$_5$ stoichiometry and structure belonging to orthorhombic space group *Cmc*2$_1$ (space group n. 36).

Relevant refinement parameters are reported in Table 1 for one of the investigated sample points, whereas the cif file of the solved crystal structure of Sb$_3$N$_5$, containing the supplementary crystallographic data for this paper, has been deposited in the CSD CCDC-ICSD database under Deposition Number 2301543. These data are provided free of charge by the joint Cambridge Crystallographic Data Centre and Fachinformationszentrum Karlsruhe Access Structures service.

As far as we know, the observation of the *Cmc*2$_1$ structure of Sb$_3$N$_5$, which was consistently determined in several points across the same sample and in different samples, represents the experimental evidence for the existence of a long sought-after crystalline nitride of antimony. It is worth to mention that the crystal structure of Sb$_3$N$_5$ was observed to persist at the pressure of synthesis
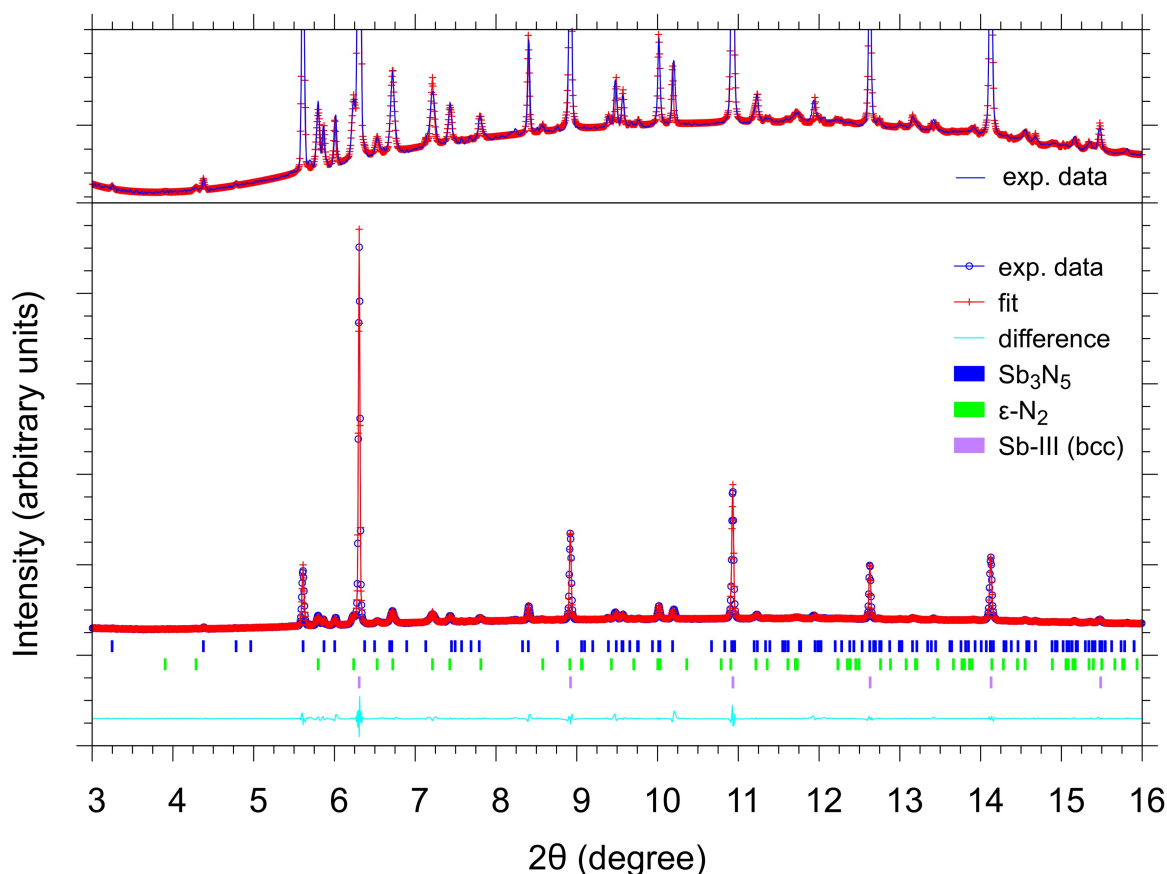

Figure 2. Lower panel: Pawley fit of a panoramic XRD pattern ($\lambda = 0.2647$ Å) acquired in one of the sample points at the center of the laser heated area at 33 GPa and room T after LH, showing the presence of Sb$_3$N$_5$ (*Cmc*2$_1$) and of excess crystalline ε-N$_2$[38] and unreacted Sb-III (bcc).[37] Upper Panel: zoom of the experimental pattern shown in the lower panel.

Table 1: Selected refinement parameters and atomic coordinates for the crystal structure of Sb_3N_5 at 35.0 GPa and room T. *m*, *i*, *o* respectively indicate measured, independent and observed reflections.

Chemical formula	Sb_3N_5		
Formula Weight	435.30		
Pressure (GPa)	35.0		
Temperature (K)	293(2)		
Crystal system	Orthorhombic		
Space group	$Cmc2_1$ (n. 36)		
a (Å)	12.305(7)		
b (Å)	5.0531(7)		
c (Å)	5.1945(7)		
α (°)	90		
β (°)	90		
γ (°)	90		
V (Å³)	323.0(2)		
Z (formula units)	4		
density (g cm⁻³)	8.952		
Wavelength (Å)	0.3738		
No. of m / i / o [I > 2σ(I)] reflections	289, 222, 216		
R_{int}	0.026		
Final R indices [I > 2 σ(I)]	R1 = 0.0537, wR2 = 0.1385		
Final R indices [all data]	R1 = 0.0541, wR2 = 0.1387		
S (goodness of fit)	1.15		
No. of parameters	19		
Atom (Wyckoff site)	Coordinates		
	x	y	z
Sb01 (8b)	0.6642(3)	0.7552(3)	0.2771(6)
Sb02 (4a)	0.5	0.7233(5)	0.7232(4)
N01 (4a)	0.5	0.896(8)	0.365(7)
N02 (8b)	0.600(5)	0.550(4)	-0.009(4)
N03 (8b)	0.693(5)	0.115(6)	0.151(4)

without decomposition, indicating Sb_3N_5 to be stable or metastable at ~ 35 GPa and room T conditions.

The $Cmc2_1$ structure, obtained by single-crystal data, was used for the multi-phase Pawley fit of the panoramic XRD pattern acquired on a different sample of Sb and N_2 laser heated at comparable HP-HT conditions and containing, besides Sb_3N_5, also unreacted bcc Sb-III and ε-N_2. The agreement of the fit with the experimental data is shown in Figure 2.

The asymmetric unit of crystalline Sb_3N_5 ($Cmc2_1$) contains two types of independent Sb atoms (Sb01 and Sb02) and three types of independent N atoms (N01, N02 and N03), respectively located on Wyckoff positions 8b (Sb01), 4a (Sb02), 4a (N01), 8b (N02) and 8b (N03).

The analysis of the interatomic distances and angles indicates that every Sb is coordinated by N atoms and vice versa. Only chemical bonds between Sb and N are present in the connection scheme of Sb_3N_5, indicating the complete cleavage of the N≡N triple bond, without formation of azides, diazenides and pernitrides units or polynitrogen chains. A complete list of the bond lengths and angles is reported in Table SI-1. According to the van Arkel-Ketelaar triangle, requiring a (Pauling) electronegativity (χ) difference $\triangle\chi > 1.7$ for ionicity in binary compounds,[39] the relatively small value of $\triangle\chi = 0.99$ between Sb ($\chi_{Sb} = 2.05$) and N ($\chi_N = 3.04$) indicates a covalent rather than ionic nature of Sb_3N_5. Even if these electronegativity values refer

to ambient pressure, no significant effect is expected at the experimental pressures of this study.[40]

Both types of Sb atoms (Sb01 and Sb02) have six N atoms as nearest neighbors, forming SbN_6 units, which exhibit different coordination geometry. Whereas Sb01 atoms are indeed hexa-coordinated, adopting a distorted octahedral coordination with Sb–N distances ranging between 1.97(3) and 2.189(16) Å and N–Sb–N angles between 77.2(18) and 108.0(11)° (equatorial-equatorial and axial-equatorial) (Table SI-1 and Figure 3G), the Sb02 atoms are instead hexa-coordinated in a trigonal prismatic coordination, with Sb–N distances ranging between 2.05(4) and 2.21(4) Å and N–Sb-N angles between 74.4(6) and 99.0(11)° (Table SI-1 and Figure 3H).

In the case of the Sb02 atoms, two additional N atoms are located at longer distance (2.54(6) Å), suggesting the occurrence of weaker secondary bonding interactions and an increase in the coordination number of the Sb02 atoms from 6 to 8[41] (Table SI-1 and Figure 3J), ultimately leading to SbN_8 units in square antiprismatic coordination (SAPR-8)[42] and possibly becoming more evident at higher pressure.

Of the three types of N atoms, N01 has four nearest neighbor Sb atoms (2 Sb01 and 2 Sb02), forming NSb_4 units in a distorted tetrahedral coordination with two N01-Sb01 distances of 2.192 Å and two N01-Sb02 distances of 2.055 and 2.061 Å (Table SI-1 and Figure 3L).

The N02 atoms have four nearest neighbor Sb atoms (2 Sb01 and 2 Sb02), forming NSb_4 units too, but in severely distorted tetrahedral coordination, with N02-Sb distances ranging between 1.98 and 2.21 Å and the off-center Sb02 almost lying on the plane defined by three Sb atoms (Sb01, Sb01 and Sb02) (Table SI-1 and Figure 3M).

Finally the N03 atoms have three nearest neighbor Sb atoms (Sb01), with N03-Sb01 distances ranging between 1.97(3) and 2.08(2) Å, in trigonal pyramidal coordination (Table SI-1 and Figure 3N), and a fourth next nearest neighbor Sb atom (Sb02) at a N03-Sb02 distance of 2.54 (6) Å, which, according to the square antiprismatic coordination of the Sb02 atoms, leads to a distorted $N03Sb_4$ tetrahedral coordination of the N03 atoms (Table SI-1 and Figure 3O).

Adopting the same notation used to describe phosphorus nitrides,[4,5,8] the structure of Sb_3N_5 can be represented in terms of polyhedral symbols as ${}^3_\infty[Sb_2^{[6o]} Sb_1^{[8acb]} N_1^{[4t]} N_1^{[4t]} N_1^{[4t]}]$ (or as ${}^3_\infty[Sb_2^{[6o]} Sb_1^{[6p]} N_1^{[4t]} N_1^{[4t]} N_1^{[3n]}]$ if adopting the SbN_6 trigonal prismatic description for the coordination of the Sb02 atoms), where ${}^3_\infty[\cdots]$ indicates an infinite 3D polymeric network of polyhedra, and the subscripts and superscripts of each element respectively denote the number of atoms of the element and its coordination number. The letters in the superscripts indicate: *o* octahedral coordination, *acb* square anti-prismatic coordination, *p* trigonal prismatic coordination, *t* tetrahedral coordination, *n* an electron lone pair.[42–44]

Details of the crystal structure highlighting the two additional Sb···N distances with respect to the trigonal prismatic coordination are shown in panels J and K.

Experimental structural data about bond lengths in crystalline compounds of Sb and N available in literature are essentially limited to antimony triazide $Sb(N_3)_3$ (2.119(4)-

Angew. Chem. Int. Ed. **2024**, e202319278 (5 of 11)

© 2023 The Authors. Angewandte Chemie International Edition published by Wiley-VCH GmbH
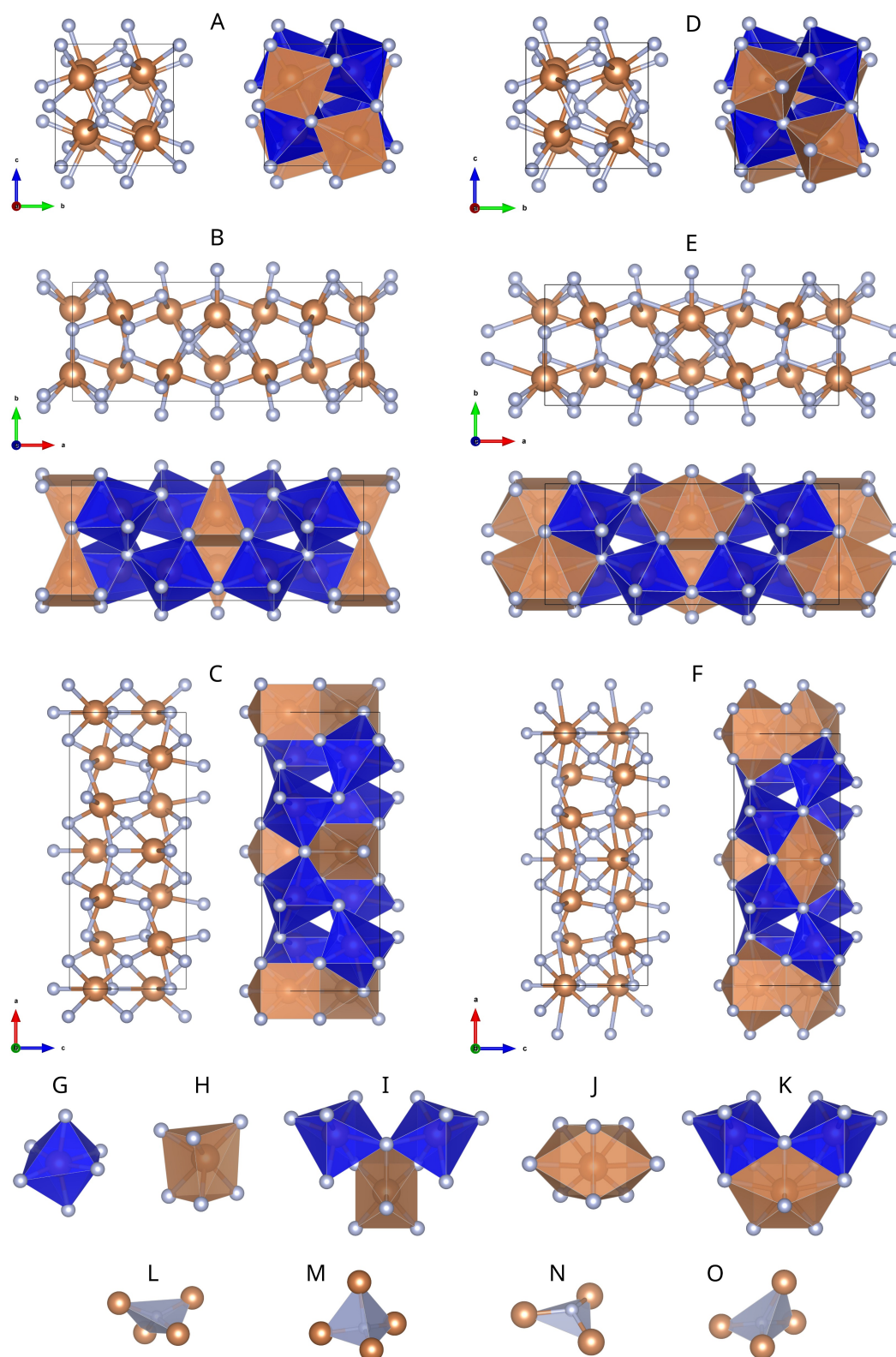
Figure 3. Ball-and-stick and polyhedron views of the unit cell structure of Sb_3N_5 at 35.0 GPa and room T along different crystallographic directions obtained by single crystal synchrotron XRD at 35 GPa and room T, represented according to a cutoff Sb—N bond length of 2.50 Å (panels A, B, C, G, H and I), leading to $Sb01N_6$ octahedra (blue) and $Sb02N_6$ trigonal prisms (orange), and to a cutoff Sb—N bond length of 2.54 Å (panels D, E, F, J and K), leading to $Sb01N_6$ octahedra (blue) and $Sb02N_8$ square antiprisms (orange), which include the two Sb02-N03 distances at 2.54 Å. The NSb_4 distorted tetrahedra at N01 (L, $N01Sb_4$) and N02 (M, $N02Sb_4$) and the NSb_3 trigonal pyramids at N03 (N, $N03Sb_3$), also becoming distorted NSb_4 tetrahedra when including the 2.54 Å N03-Sb02 distance (O, $N03Sb_4$), are represented by gray polyhedra. Sb and N atoms are represented by orange and gray spheres, respectively. The two additional Sb···N distances with respect to the trigonal prismatic coordination are highlighted in panels J and K.

2.151(5) Å),[27,28] to the $[Sb(N_3)_4]^-$ (2.071-2.280 Å),[29] [Sb-$(N_3)_5]^{2-}$ (2.099(2)-2.324(2) Å),[45] and $[Sb(N_3)_6]^-$ (2.065(2)-2.085(2) Å)[45,46] anions, to the neutral base stabilized dmap-$Sb(N_3)_5$ compound (2.0636-2.1366 Å, dmap=4-dimethylaminopyridine)[47] and to Zn_2SbN_3 (1.990-2.068 Å)[15] at ambient pressure.

As expected from the involvement of the electron lone pair in the chemical bond formation, the Sb–N distances in Sb_3N_5, ranging from 1.97 to 2.21 Å (Table SI-1), are consistent with the available experimental and calculated literature data at ambient pressure (section SI-3), with the single bond length values estimated from the sum of the calculated covalent radii of Sb and N (~2.1 Å) at ambient pressure[48] and with recently synthesized $SbCN_3$ at high pressure (2.0179 Å at 32.7 GPa, 2.022 Å at 32.8 GPa).[34]

The Sb–N bond lengths in Sb_3N_5 are also in agreement with the Sb–N bond lengths of the antimony nitride crystalline structures calculated by Lian *et al.*[33] at high pressure: 2.105-2.153 Å for $C2/m$ SbN_2-I at 20 GPa, 2.092-2.168 Å for $C2/m$ SbN_2-II at 40 GPa, 2.105-2.208 Å for $C2/m$ SbN_4-I at 20 GPa and 2.052-2.183 Å for $P\bar{1}$ SbN_4-II at 40 GPa.

However, Sb–N distances ranging between 2.35 and 2.56 Å at ambient pressure, comparable to our Sb02-N03 distances of 2.54 Å at 35 GPa, have been reported in the $(PNP)_2[Sb(pc^{2-})_2]Br\cdot2$ Et_2O complex of Sb(V) (PNP= triphenylphosphine, pc=phthalocyaninate), where Sb exhibits square antiprismatic coordination by eight N atoms, four of which are located on one of two crown ether like chelating rings and four on the other.[49]

Considering a cutoff Sb–N single-bond length of 2.50 Å, well beyond the longest experimentally reported Sb–N single bond length of 2.324(2) at ambient pressure ([Sb-$(N_3)_5]^{2-}$)[45] in non-chelating ligands, and thus excluding the two Sb02-N03 distances of 2.54 Å (Table SI-1), the crystalline structure of Sb_3N_5 can be described in terms of polyhedra as made of octahedral and trigonal prismatic SbN_6 units, respectively involving the Sb01 and Sb02 atoms, of NSb_4 distorted tetrahedra, respectively involving the N01 and N02 atoms, and of NSb_3 trigonal pyramids, involving the N03 atoms, which are illustrated in Figure 3 (panels A, B, C, G, H, I, L, M and N).

Overall, considering all the experimental Sb–N nearest neighbor distances and thus including also the two Sb02-N03 distances of 2.54 Å (Table SI-1), the polyhedra involving the Sb02 atoms can be described as SbN_8 square antiprismatic units (Figure 3, panels D, E, F, J and K) and those involving the N03 atoms as distorted NSb_4 tetrahedra (Figure 3, panel O). Interestingly, in spite of tetrahedral SbN_4 being reported in Zn_2SbN_3[15] at ambient conditions, the fact that no tetrahedral four-coordination of Sb is observed in Sb_3N_5 at 35 GPa may be related to the effect of pressure in stabilizing higher coordination numbers,[41] as also confirmed by the report of octahedrally coordinated Sb^{5+} in $SbCN_3$, where Sb^{5+} is hexacoordinated by the N atoms belonging to six guanidinate ($[CN_3]^{5-}$) ions.[34]

The high-pressure chemistry of Sb with N can be compared to that of P[6–8] and As.[9]

The framework of chemical bonding connecting Sb and N in Sb_3N_5 markedly differs from the connection scheme of lighter As with N in AsN,[9] synthesized (>25 GPa, >1400 K) and structurally characterized (28–40 GPa, room T) at comparable pressure conditions, which appears instead similar to that of cubic gauche N (cg-N).[50] Whereas As prefers the oxidation state +3 with coordination number 3 in trigonal pyramidal coordination and electron lone pair expression, Sb adopts instead the oxidation state +5, with coordination number 6 and 8, respectively in octahedral and square antiprismatic coordination (or coordination number 6 in octahedral and trigonal prismatic coordination, according to the structure description with 2.50 Å cutoff Sb–N bond length).

From this point of view, the structural and chemical behavior of Sb with N rather appears closer to that of P, the second element in group 15, in δ-P_3N_5, at much higher pressure (72 and 118 GPa).[8] Indeed clear similarities emerge when comparing the crystalline structures of Sb_3N_5 ($Cmc2_1$, space group n. 36) and recently discovered δ-P_3N_5 ($C2/c$, space group n. 15).[8]

The two crystalline nitrides have the same stoichiometry and, similarly to δ-P_3N_5, which features two types of P atoms, also Sb_3N_5 contains two types of Sb atoms. Furthermore, in both cases all the P and Sb atoms are at least hexacoordinated, respectively forming PN_6 and SbN_6 or SbN_8 units.

Nevertheless, whereas in δ-P_3N_5 only octahedral PN_6 units are present on both Wyckoff sites (8f and 4a), in Sb_3N_5 the coordination polyhedra formed by the two types of Sb atoms, located on 8b and 4a Wyckoff sites, respectively exhibit octahedral SbN_6 and square antiprismatic SbN_8 (or trigonal prismatic SbN_6) coordination.

Furthermore, in δ-P_3N_5 the three types of N atoms occupy different Wyckoff positions, respectively forming tetrahedral NP_4 (4e and 8f) and trigonal pyramidal NP_3 (8f) units. A similar occurrence is found in Sb_3N_5, where the three types of N atoms occupy the 4a (N01), 8b (N02) and 8b (N03) Wyckoff positions, adopting distorted tetrahedral NSb_4 coordination as $N01Sb_4$, $N02Sb_4$ and $N03Sb_4$ units, with the last ones exhibiting one markedly longer N03-Sb02 distance (2.54 Å) and actually becoming $N03Sb_3$ trigonal pyramidal when adopting a 2.50 Å cutoff distance for the Sb–N bond.

Within this assumption, in both cases 2/3 of the N atoms are four coordinated in a fully saturated tetrahedral coordination, whereas 1/3 of the N atoms is three-coordinated and likely hosts an electron lone pair.

Noticeably, the existence of tetrahedral coordination of N, firstly reported in δ-P_3N_5 for P nitrides, is here confirmed for Sb in Sb_3N_5. As suggested for the formation of tetrahedral NP_4 units in δ-P_3N_5,[8] also in Sb_3N_5 the presence of tetrahedral NSb_4 units may likely be explained by the pressure induced formation of a dative bonding involving the electron lone pairs of N atoms and one of the surrounding Sb atoms.

According to *ab initio* molecular dynamics simulations, the local formation of four-coordinated NSb_4 tetrahedra sharing corners or edges seems to drive the bonding mechanism of N to Sb in amorphous N-doped Sb, persisting

also after crystallization and apparently representing an important feature in phase change materials performances of N-doped amorphous Sb.[12,13]

Within this scenario, the existence and evolution with pressure of the trigonal prismatic hexa-coordination into a square antiprismatic octa-coordination, including the two additional distances in the coordination sphere, represents a unique feature among crystalline pnictogen nitrides.

Interestingly, although not pointed out by Lian *et al.* in their paper, a similar occurrence can be found in the predicted Sb_2N_3 structure (*Cmcm*) at 120 GPa.[33] In this calculated structure one of the two types of Sb atoms exhibits octahedral SbN_6 coordination, whereas the second one has six nearest neighbor N atoms in trigonal prismatic coordination at distances between 2.016 and 2.191 Å and two additional second nearest neighbor N atoms at 2.318 Å.

Despite the significantly higher pressure of the calculated structure, the coordination of the Sb atoms in Sb_2N_3 appears fully consistent with the coordination of Sb in the experimental Sb_3N_5 structure reported here.

On other side, no SbN_3 units in trigonal pyramidal coordination are here found in Sb_3N_5, as instead observed in the calculated SbN_2-I and SbN_4-II structures at high pressure[33] and in the proposed structure of the transient SbN compound observed by Chen *et al.* at ambient pressure and high temperature during RTA.[32]

Another common feature, relating Sb_3N_5 and δ-P_3N_5, is the presence of characteristic structural motifs made of polyhedra connected through shared vertexes and edges.

Whereas in δ-P_3N_5 these motifs consist of linear chains of single vertex-sharing PN_6 octahedra formed by one of the two types of P atoms and of chains of edge- and face-sharing double PN_6 octahedra involving the other type of P atoms, the crystal structure of Sb_3N_5 can be viewed as the ordered stacking in the *bc* plane of bi-layers of vertex sharing SbN_6 octahedra alternated to mono-layers of vertex- and edge-sharing SbN_8 square antiprisms (Figure 4A–H). The mono-layers can be alternatively described in terms of trigonal prismatic SbN_6 polyhedra, depending on the selected cutoff distance for the Sb–N bond (Figure SI-1). Within the bi-layer, every SbN_6 octahedron is connected by shared vertexes to eight octahedra in the same bilayer (Figure 4B and 4E), whereas within the monolayer, every SbN_8 square antiprism (SbN_6 trigonal prism) is connected to four other polyhedra of the same type, sharing the two opposite edges of one square face with two of them and the two vertexes opposite to the shared edges with the remaining two of them (Figure 4C and 4F and Figure SI-1). The bi-layers of octahedra and the mono-layers of square antiprisms (trigonal prisms) are connected with each other by shared vertexes and edges.

Interestingly, the electron lone pairs of two N03 atoms, belonging to the two bi-layers of SbN_6 octahedra on the opposite sides of a trigonal prism monolayer, appear to have favorable orientation to interact with the same Sb02 atom through the square faces of the corresponding SbN_6 trigonal prism (Figure 3, panel I). The two N03···Sb02 distances correspond indeed to the two additional 2.54(6) Å distances leading to square antiprismatic coordination of the Sb02

atoms (Figure 3, panels J and K), which is possibly further favored at higher pressure.

Overall, from a chemical point of view, these are relevant pieces of information, providing insight on bond theory of pnictogens under high density conditions, particularly concerning the progressive evolution with pressure of non-bonding electron lone pairs into bonding interactions. The processes of bond formation through the progressive strengthening of weaker secondary bonding interactions represents a relevant topic in bond theory description.[41]

A similar occurrence has been observed for example in the inter-layer bond formation mechanism during the A7 to simple cubic phase transition in P, leading to the discovery of the pseudo simple-cubic (p-sc) structure.[51,52]

Conclusion

In this study we report the direct chemical reaction of Sb and N_2 under HP-HT conditions generated by a laser heated DAC, leading to the synthesis of crystalline Sb_3N_5 according to the following chemical equation:

$$3\,Sb + \frac{5}{2}N_2 \xrightarrow[T=1600-2200\,K]{P>32.0\,GPa} Sb_3N_5 \qquad (1)$$
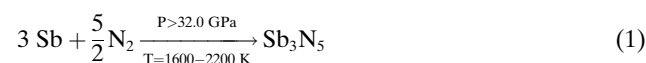
The $Cmc2_1$ crystal structure of Sb_3N_5, was determined at high pressure and ambient temperature using synchrotron XRD and its persistence without decomposing indicates thermodynamic or meta- stability at the experimental conditions, in agreement with theoretical prediction suggesting the existence of metastable crystalline pnictogen nitrides.

From a chemical point of view, the discovery of crystalline Sb_3N_5 not only represents a landmark in the chemistry of Sb and N, but also sets a milestone along the road to the exploration of crystalline pnictogen nitrides, expanding the family of these so far elusive compounds to the fifth period of the periodic table of the elements and possibly paving the way to the discovery of other structures and stoichiometries in the Sb–N system. In a broader perspective, the structural characterization of Sb_3N_5 provides new insights about fundamental aspects of pnictogens chemistry with respect to the crystalline nitrides of lighter P and As known so far, marking a significant advancement in the knowledge of crystalline nitrides of group 15 elements and possibly leading to the high-pressure synthesis and discovery of an entire class of new pnictogen nitrides with different structures, stoichiometry and multivalent composition. Implications concern new advanced and innovative materials of energetic and technological relevance potentially recoverable to ambient conditions as stable or metastable systems, like phase change materials, layered compounds and high energy density N-rich materials.
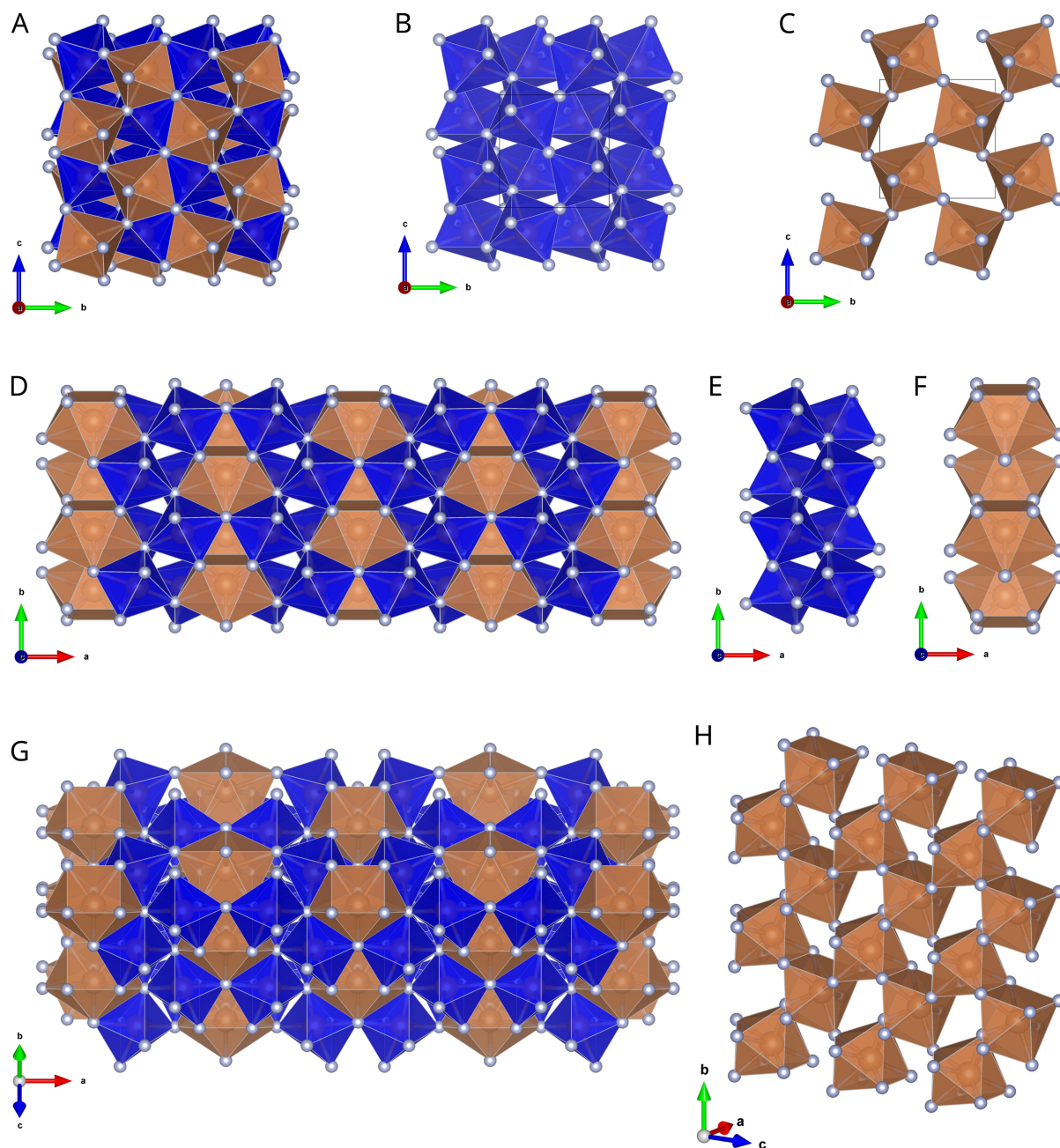
Figure 4. Polyhedron views of the unit cell structure of Sb_3N_5 at 35.0 GPa and room T along different crystallographic directions obtained by single crystal synchrotron XRD (panels A, D, G) highlighting the presence of bi-layers of $Sb01N_6$ octahedra (panels B, E) and of layers of $Sb02N_8$ square-antiprisms (panels C, F, H). Sb and N atoms are represented by orange and gray spheres, respectively. The distorted octahedral SbN_6 and square antiprismatic SbN_8 units are represented as blue and orange polyhedra, respectively. The cutoff Sb–N bond length has been set to 2.54 Å. An alternative view obtained with a cutoff Sb–N bond length of 2.50 Å, excluding the two Sb02-N03 bond lengths at 2.54 Å and leading to a structure description in terms of $Sb02N_6$ trigonal prisms, is shown in Figure SI-1.

Supporting Information

Experimental details, additional data and comments are provided in the Supporting Information.

Acknowledgements

Conflict of Interest

The authors declare no competing interests.

Data Availability Statement

Data are associated to DOI 10.15151/ESRF-ES-735695383 and 10.15151/ESRF-ES-1100171991, according to the ESRF data policy.

[1] W. Schnick, *Angew. Chem. Int. Ed.* **1993**, *32*, 806–818.

[2] D. H. Gregory, *J. Chem. Soc. Dalton Trans.* **1999**, 259–270.

[3] O. C. Gagné, *Chem. Sci.* **2021**, *12*, 4599–4622.

[4] S. Horstmann, E. Irran, W. Schnick, *Angew. Chem. Int. Ed.* **1997**, *36*, 1873–1875.

[5] K. Landskron, H. Huppertz, J. Senker, W. Schnick, *Angew. Chem. Int. Ed.* **2001**, *40*, 2643–2645.

[6] K. Niwa, Y. Iijima, M. Ukita, R. Toda, K. Toyoura, T. Sasaki, K. Matsunaga, N. A. Gaida, M. Hasegawa, *J. Raman Spectrosc.* **2021**, *52*, 1064–1072.

[7] M. Ceppatelli, D. Scelta, M. Serrano-Ruiz, K. Dziubek, F. Izquierdo-Ruiz, J. M. Recio, G. Garbarino, V. Svitlyk, M. Mezouar, M. Peruzzini, R. Bini, *Inorg. Chem.* **2022**, *61*, 12165–12180.

[8] D. Laniel, F. Trybel, A. Néri, Y. Yin, A. Aslandukov, T. Fedotenko, S. Khandarkhaeva, F. Tasnádi, S. Chariton, C. Giacobbe, E. L. Bright, M. Hanfland, V. Prakapenka, W. Schnick, I. A. Abrikosov, L. Dubrovinsky, N. Dubrovinskaia, *Chem. Eur. J.* **2022**, *28*, e202201998.

[9] M. Ceppatelli, D. Scelta, M. Serrano-Ruiz, K. Dziubek, M. Morana, V. Svitlyk, G. Garbarino, T. Poręba, M. Mezouar, M. Peruzzini, R. Bini, *Angew. Chem. Int. Ed.* **2022**, *61*, e202114191.

[10] W. Sun, S. T. Dacek, S. P. Ong, G. Hautier, A. Jain, W. D. Richards, A. C. Gamst, K. A. Persson, G. Ceder, *Sci. Adv.* **2016**, *2*, 1–8 e1600225.

[11] W. Sun, A. Holder, B. Orvañanos, E. Arca, A. Zakutayev, S. Lany, G. Ceder, *Chem. Mater.* **2017**, *29*, 6936–6946.

[12] Y. Hu, X. Zhu, H. Zou, J. Zhang, L. Yuan, J. Xue, Y. Sui, W. Wu, S. Song, Z. Song, *Appl. Phys. Lett.* **2016**, *108*, 223103.

[13] Y. Sun, C. Yu, X. Zhu, H. Zou, Y. Hu, M. Pei, L. Zhai, Y. Sui, W. Wu, Z. Song, *J. Phys. D* **2019**, *52*, 455107.

[14] L. Prazakova, E. Nolot, E. Martinez, D. Rouchon, N. Rochat, C. Sabbione, J. Li, D. Eichert, G. Pepponi, M. Bernard, G. Navarro, *J. Appl. Phys.* **2022**, *132*, 205102.

[15] E. Arca, J. D. Perkins, S. Lany, A. Mis, B.-R. Chen, P. Dippo, J. L. Partridge, W. Sun, A. Holder, A. C. Tamboli, M. F. Toney, L. T. Schelhas, G. Ceder, W. Tumas, G. Teeter, A. Zakutayev, *Mater. Horiz.* **2019**, *6*, 1669–1674.

[16] K. N. Heinselman, S. Lany, J. D. Perkins, K. R. Talley, A. Zakutayev, *Chem. Mater.* **2019**, *31*, 8717–8724.

[17] C. Liu, W. Wan, J. Ma, W. Guo, Y. Yao, *Nanoscale* **2018**, *10*, 7984–7990.

[18] M. Kolos, R. Verma, F. Karlický, S. Bhattacharya, *J. Phys. Chem. C* **2022**, *126*, 14931–14959.

[19] Y. Zhang, T. Ouyang, C. He, J. Li, C. Tang, *Nanoscale* **2023**, *15*, 6363–6370.

[20] Y. Zhang, C. Cui, T. Ouyang, C. He, J. Li, M. Chen, C. Tang, *Appl. Phys. Lett.* **2023**, *122*, 182204.

[21] N. H. Coy, H. Sponer, *Phys. Rev.* **1938**, *53*, 495–495.

[22] N. H. Coy, H. Sponer, *Phys. Rev.* **1940**, *58*, 709–713.

[23] T. Shiraishi, Y. Arai, S. Yamazaki, *J. Non-Cryst. Solids* **1985**, *77–78*, 1313–1316.

[24] Q. Sun, W.-J. Li, Z.-W. Fu, *Solid State Sci.* **2010**, *12*, 397–403.

[25] C. M. Caskey, R. M. Richards, D. S. Ginley, A. Zakutayev, *Mater. Horiz.* **2014**, *1*, 424–430.

[26] E. Nolot, C. Sabbione, W. Pessoa, L. Prazakova, G. Navarro, *Appl. Surf. Sci.* **2021**, *536*, 147703.

[27] R. Haiges, A. Vij, J. A. Boatz, S. Schneider, T. Schroer, M. Gerken, K. O. Christe, *Chem. Eur. J.* **2004**, *10*, 508–517.

[28] S. Schulz, B. Lyhs, G. Jansen, D. Bläser, C. Wölper, *Chem. Commun.* **2011**, *47*, 3401–3403.

[29] R. Haiges, M. Rahm, K. O. Christe, *Inorg. Chem.* **2013**, *52*, 402–414.

[30] W. Sun, C. J. Bartel, E. Arca, S. R. Bauers, B. Matthews, B. Orvañanos, B.-R. Chen, M. F. Toney, L. T. Schelhas, W. Tumas, J. Tate, A. Zakutayev, S. Lany, A. M. Holder, G. Ceder, *Nat. Mater.* **2019**, *18*, 732–739.

[31] A. Mis, S. Lany, G. L. Brennecka, A. Tamboli, *J. Mater. Chem. C* **2021**, *9*, 13904–13913.

[32] B.-R. Chen, S. Lany, L. L. Kelly, E. Arca, Y. Iguchi, J. D. Perkins, H. Yanagi, M. F. Toney, L. T. Schelhas, A. Zakutayev, *Cell Rep. Phys. Sci.* **2022**, *3*, 100980.

[33] L. Lian, Y. Liu, D. Li, S. Wei, *RSC Adv.* **2020**, *10*, 2448–2452.

[34] L. Brüning, N. Jena, E. Bykova, P. L. Jurzick, N. T. Flosbach, M. Mezouar, M. Hanfland, N. Giordano, T. Fedotenko, B. Winkler, I. A. Abrikosov, M. Bykov, *Angew. Chem. Int. Ed.* **2023**, *62*, e202311519.

[35] A. L. Coleman, M. G. Gorman, R. Briggs, R. S. McWilliams, D. McGonegle, C. A. Bolme, A. E. Gleason, D. E. Fratanduono, R. F. Smith, E. Galtier, H. J. Lee, B. Nagler, E. Granados, G. W. Collins, J. H. Eggert, J. S. Wark, M. I. McMahon, *Phys. Rev. Lett.* **2019**, *122*, 255704.

[36] G. Weck, F. Datchi, G. Garbarino, S. Ninet, J.-A. Queyroux, T. Plisson, M. Mezouar, P. Loubeyre, *Phys. Rev. Lett.* **2017**, *119*, 235701.

[37] K. Aoki, S. Fujiwara, M. Kusakabe, *Solid State Commun.* **1983**, *45*, 161–163.

[38] H. Olijnyk, *J. Chem. Phys.* **1990**, *93*, 8968–8972.

[39] D. Shriver, M. Weller, T. Overton, J. Rourke, F. Armstrong, *Inorganic Chemistry*, W. H. Freeman, 6th ed., **2014**.

[40] M. Rahm, R. Cammi, N. W. Ashcroft, R. Hoffmann, *J. Am. Chem. Soc.* **2019**, *141*, 10253–10271.

[41] W. Grochala, R. Hoffmann, J. Feng, N. Ashcroft, *Angew. Chem. Int. Ed.* **2007**, *46*, 3620–3642.

[42] N. G. Connelly, T. Damhus, R. M. Hartshorn, A. T. Hutton, *Nomenclature of Inorganic Chemistry, IUPAC RECOMMENDATIONS 2005*, RSC Publishing, 1st ed., **2005**.

[43] J. Lima-de-Faria, E. Hellner, F. Liebau, E. Makovicky, E. Parthé, *Acta Crystallogr. Sect. A* **1990**, *46*, 1–11.

[44] U. Müller, *Inorganic Structural Chemistry*, John Wiley & Sons Ltd, 2nd ed., **2006**.

[45] B. Lyhs, G. Jansen, D. Bläser, C. Wölper, S. Schulz, *Chem. Eur. J.* **2011**, *17*, 11394–11398.

[46] R. Haiges, J. A. Boatz, A. Vij, V. Vij, M. Gerken, S. Schneider, T. Schroer, M. Yousufuddin, K. O. Christe, *Angew. Chem. Int. Ed.* **2004**, *43*, 6676–6680.

[47] B. Lyhs, D. Bläser, C. Wölper, S. Schulz, G. Jansen, *Inorg. Chem.* **2012**, *51*, 5897–5902.

[48] P. Pyykkö, M. Atsumi, *Chem. Eur. J.* **2009**, *15*, 12770–12779.

[49] H. Hückstädt, A. Tutaß, M. Göldner, U. Cornelissen, H. Homborg, *Z. Anorg. Allg. Chem.* **2001**, *627*, 485–497.

[50] M. I. Eremets, A. G. Gavriliuk, I. A. Trojan, D. A. Dzivenko, R. Boehler, *Nat. Mater.* **2004**, *3*, 558–563.

[51] D. Scelta, A. Baldassarre, M. Serrano-Ruiz, K. Dziubek, A. B. Cairns, M. Peruzzini, R. Bini, M. Ceppatelli, *Angew. Chem. Int. Ed.* **2017**, *56*, 14135–14140.

[52] D. Scelta, A. Baldassarre, M. Serrano-Ruiz, K. Dziubek, A. B. Cairns, M. Peruzzini, R. Bini, M. Ceppatelli, *Chem. Commun.* **2018**, *54*, 10554–10557.

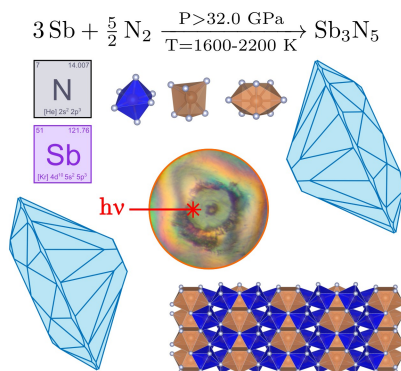## Research Articles

Nitrides

M. Ceppatelli,* M. Serrano-Ruiz,
M. Morana, K. Dziubek, D. Scelta,
G. Garbarino, T. Poręba, M. Mezouar,
R. Bini, M. Peruzzini ——— **e202319278**

High-pressure and high-temperature synthesis of crystalline Sb₃N₅

$$3\,Sb + \frac{5}{2}\,N_2 \xrightarrow[T=1600\text{-}2200\ K]{P>32.0\ GPa} Sb_3N_5$$

hν

Crystalline Sb₃N₅ has been synthesized from the high-pressure and high-temperature chemical reaction of antimony and nitrogen in a laser heated diamond anvil cell. The *Cmc*2₁ structure of Sb₃N₅, determined by single crystal synchrotron X-ray diffraction, contains two types Sb atoms in octahedral and trigonal prismatic (square antiprismatic) coordination, respectively forming alternated double- and mono-layers stacked in the *bc* plane.